PCCP

PAPER

View Article Online
View Journal | View Issue

Cite this: *Phys. Chem. Chem. Phys.*, 2024, **26**, 18138

Ligand field theory, Pauli shields and ultra-covalency in organometallic chemistry†

Robert J. Deeth

This paper explores the ligand field picture applied to organometallic compounds. Given the dearth of experimental data, the high-level *ab initio* ligand field theory (aiLFT) method is deployed as a surrogate for experiment and the necessary d orbital sequences and relative energies are obtained computationally. These are fitted to local cellular ligand field (CLF) σ, π and δ bonding parameters. Results are reported for planar $[Cu(CR_3)_4]^-$, (R = F, H), octahedral $M(CO)_6^n$ (M = Fe, Mn, Cr, V, Ti; n = +2, +1, 0, −1, −2), and the sandwich compounds $M(Cp)_2$ (Cp = cyclopentadienyl, M = Fe, Ni, V), $[Ni(Cp)_2]^{2+}$ and $Cr(C_6H_6)_2$. With respect to the aiLFT framework, these organometallic systems behave just like coordination complexes and most maintain the integrity of their formal d^n configurations. Both $[Cu(CR_3)_4]^-$ compounds are formulated as low-spin d^8 Cu^{III} species and have normal ligand fields consistent with their planar geometries. The metal carbonyls reveal a new way of counting valence electrons which only requires the CLF d orbital energy level diagram to rationalise the 18-electron rule as well as its many exceptions. The bonding in sandwich compounds shows a remarkable variation. In ferrocene, Cp^- behaves as a strong field ligand, comparable to $[CN]^-$ in $[Fe(CN)_6]^{4-}$. $Fe(Cp)_2$ is low spin as is $Cr(C_6H_6)_2$. Cp^- in $Fe(Cp)_2$ is a weak σ donor, strong π donor and weak δ acceptor while benzene in $Cr(C_6H_6)_2$ is also a weak σ and strong π donor but is a much better δ acceptor. In contrast, Cp^- is weak field in high spin, 20-electron $Ni(Cp)_2$ but 'ultra-covalent' in $[Ni(Cp)_2]^{2+}$. The formal IV oxidation state is too high for the ligand set and the integrity of the d^6 configuration is lost. Similarly, $[V(CO)_6]^-$ and $[Ti(CO)_6]^{2-}$ are ultra-covalent except now the formal metal oxidation states are too negative. Both mechanisms relate to the breaching of the metal's $3s^23p^6$ 'Pauli shield' and these ultra-covalent systems lie outside the *ab initio* ligand field regime. However, within the ligand field regime, the bonding in 'coordination complexes' and 'organometallic compounds' has the same conceptual footing and the nature of the local σ, π and δ interactions can be extracted from analysing the ligand field d orbitals.

Received 21st February 2024,
Accepted 10th June 2024

DOI: 10.1039/d4cp00764f

rsc.li/pccp

1. Introduction

Ligand field theory (LFT) is one of the most enduring conceptual models in inorganic chemistry and remains a mainstay of the transition metal chemistry curriculum.[1] It emerged in the 1950s in response to the quantitative failure of the earlier electrostatic crystal field theory (CFT).[2]

In CFT, the d-orbital splitting in, for example, an octahedral crystal field of six point charges is 10Dq:

$$10\mathrm{Dq} = \frac{Ze^2\langle r_\mathrm{d}^4\rangle}{6a^5}q \qquad (1)$$

where Z is the charge on the metal ion, $\langle r_\mathrm{d}\rangle$ is its average d orbital radius, a is the distance from the metal nucleus to the point charge, and q is the magnitude of the point charge.

Attempts to compute 10Dq from first principles gave poor agreement with experiment.[3] In response, explicit calculation of the d-orbital splitting was replaced by a parametric fit to experimental data and 10Dq became the now familiar ligand field parameter Δ_oct.[4]

LFT combined the excellent symmetry treatment of CFT with the flexibility of a parametric approach and reproduced the d–d spectra and magnetic properties of d^n Werner-type complexes to good accuracy.[5] LFT was very successful and many ligand field concepts, such as the spectrochemical series, and the ligand field stabilisation energy (LFSE), entered mainstream chemical nomenclature. However, the global, symmetry-based parameters such as Δ_oct were unsatisfactory. In particular, they failed to account for how a negatively charged ligand such as fluoride could have a much smaller ligand field than neutral ligands such as ammonia or a phosphine. Mulliken's MO model suggested a resolution.

Department of Chemistry, University of Warwick, CV4 7AL, UK.
E-mail: r.j.deeth@warwick.ac.uk

† Electronic supplementary information (ESI) available: Details of the aiLFT protocol, Cartesian coordinates of all systems subjected to aiLFT analysis, and aiLFT and CLF data for selected ML_4 systems. See DOI: https://doi.org/10.1039/d4cp00764f

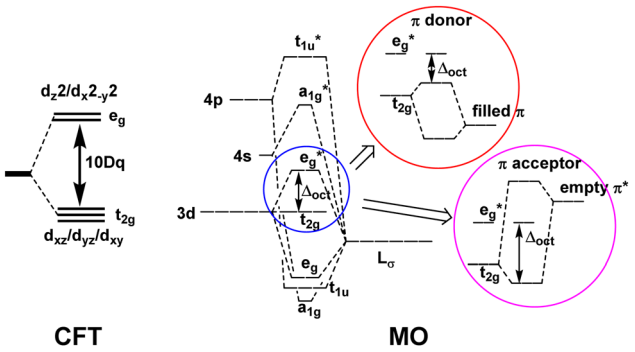

Fig. 1 A qualitative comparison of the description of the octahedral splitting given by crystal field theory (left) and by simple MO theory (right). For the latter, most textbooks focus exclusively on the $e_g^* t_{2g}$ splitting and thus only include the ligand π orbitals of t_{2g} symmetry, omitting the other 9 π orbitals.

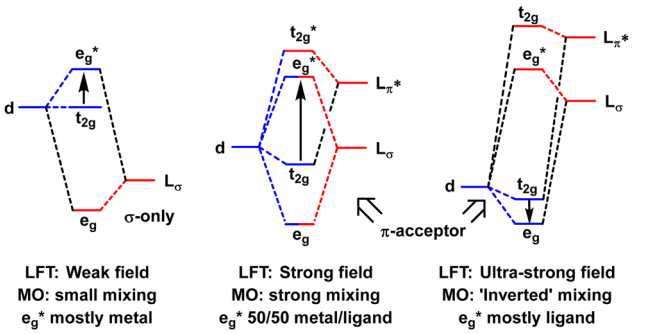

Fig. 2 Schematic depiction of the effect of progressively increasing the energies of the ligand orbitals relative to the metal d orbitals.

The qualitative MO diagram for σ-only ligands identifies Δ_{oct} as the splitting between the σ-antibonding e_g^* MOs, which are mostly metal d, and the non-bonding t_{2g} orbitals, which are 100% metal (Fig. 1, middle). By adding specific M–L π interactions – *i.e.* only the t_{2g} sets – the (partial) MO picture shows how Δ_{oct} becomes a competition between σ bonding and π bonding (Fig. 1, right). For π donors like F^- with filled, low-energy π levels, the mostly-d t_{2g}^* orbitals are destabilised, which reduces Δ_{oct}, while for π acceptor ligands, such as phosphines or CO which have empty, high-energy π orbitals, the mostly-d t_{2g} orbitals are stabilised, which tends to increase Δ_{oct}. LFT was widely viewed as an application of the MO model.[5]

However, in the early 1980s, a contrary view was put forward by Gerloch and Woolley (GW).[6–9] They formulated LFT as a projection operator approach based on the density functional theorem. The only explicit orbitals in this formulation are the metal d orbitals and all the M–L bonding interactions are implicitly accounted for in the d-orbital sequence and relative energies. These are functions of the one-electron, ligand field bonding parameters.

The most successful parameterisation schemes are the angular overlap model (AOM)[10] and the cellular ligand field (CLF) approach[6,9,11] both of which assign local σ and π bonding parameters to model each M–L interaction implicitly. For example, the d-orbital splitting in O_h systems, Δ_{oct}, is, in both AOM and CLF schemes, given by:

$$\Delta_{oct} = 3e_\sigma - 4e_\pi \qquad (2)$$

Thus, both MO and LFT models describe Δ_{oct} as a competition between σ and π bonding effects and the 'explanation' of the spectrochemical series is conceptually the same. However, the bonding is implicit in LFT, and depends on the CLF parameter values, but explicit in MO theory, and depends on orbital energies and their overlap/mixing. This leads to an interesting conceptual divergence as metal–ligand covalency increases.

In the MO model, the metal d orbitals explicitly overlap with appropriate symmetry-adapted ligand orbitals forming bonding and anti-bonding sets. Orbital overlap/mixing is the only mechanism available to alter orbital energies. At the weak-overlap extreme, the bonding set is mostly ligand while the antibonding set is mostly metal d. The latter are thus associated with the conventional 'ligand field' (Fig. 2, left). As the ligand orbitals rise relative to the metal orbitals and the covalent mixing increases, the ligand frontier orbitals eventually become higher than the metal d. The M–L interaction is now 'ultra-covalent' – *i.e.* the bonding set is mostly d while the anti-bonding set is now mostly ligand. In the octahedral model complex, the mostly-d e_g orbitals are now below the mostly-d t_{2g} orbitals implying Δ_{oct} is negative (Fig. 2, right). The ligand field is apparently 'inverted'.[12]

Based on MO calculations, an inverted ligand field has been proposed for planar $[Cu(CF_3)_4]^-$ (Fig. 3).[12,13] The mostly-d $b_{1g}(d_{x^2-y^2})$ orbital is proposed to be bonding and thus filled suggesting that a 'reduced' d^{10} Cu^I formulation with three CF_3^- and one oxidised CF_3^+ ligands is more appropriate than a low-spin d^8 Cu^{III} configuration with four CF_3^- ligands.

Of course, this analysis is model dependent and relies on the overlap mechanism inherent in MO theory. In contrast, the only explicit orbitals in the GW formulation of LFT are the metal d functions and increasing covalency simply means increasing the ligand field from weak field to strong field (Fig. 4). Δ_{oct} gets larger but the d-orbital sequence is unaltered. The GW LFT ligand field for planar $[Cu(CF_3)_4]^-$ can never invert simply by increasing σ bonding. An alternative mechanism is required.

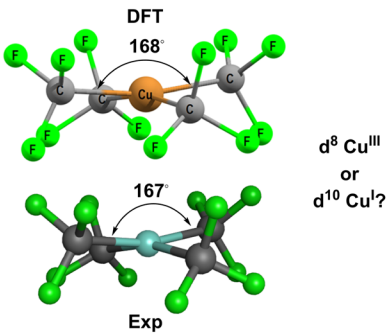

Fig. 3 Structure of $[Cu(CF_3)_4]^-$. Top: DFT-optimised. Bottom: Experimental.[14] See ESI† for further details.

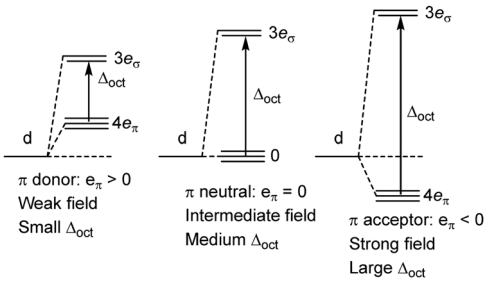

Fig. 4 Qualitative effect of increasing ligand field in the AOM/CLF bonding picture.

This paper reconciles the apparently disparate bonding pictures of MO theory and LFT by developing an equivalent ligand-field-based mechanism for internal electron transfer and exploring under what circumstances this mechanism applies. To achieve this, we address the issues of (i) what is meant by the term 'ligand field picture'; (ii) does it apply to organometallics at all and (iii) if so, how far does it extend and what insights can LFT provide into the nature of metal–ligand bonding across the whole of transition metal chemistry.

2. Theoretical and computational details

2.1. Ligand field theory

The ligand field formalism described by Gerloch and Woolley[7–9] is an example of a projection operator method. In general, each solution, E_i, of the exact Schrödinger equation, which uses the full Hamiltonian, $\mathscr{H}$, and a complete set of basis functions, $\{\Phi\}$, can be projected onto an effective Hamiltonian, $\mathscr{h}_i$, with its co-defined basis set $\{\phi_i\}$ (eqn (3)). In principle, this procedure is exact. However, as implied by the nomenclature in eqn (3), the effective Hamiltonian and its basis set are energy dependent. Each energy state requires a different Hamiltonian/basis set combination, and the process has little value.

$$E_i = \frac{\langle \Phi_i | \mathscr{H} | \Phi_i \rangle}{\langle \Phi_i | \Phi_i \rangle} = \frac{\langle \phi_i | \mathscr{h}_i | \phi_i \rangle}{\langle \phi_i | \phi_i \rangle} \qquad (3)$$

The ligand field model is a special case in that a single Hamiltonian/basis set combination can, to a reasonably good approximation, handle a range of energy states. These states are dominated by the metal d orbitals and describe the ground state magnetic properties and the d–d excitations.

The ligand field Hamiltonian, $\mathscr{h}_{\mathrm{LF}}$, (eqn (4)) comprises just three terms: the ligand field potential, V_{LF}, d–d interelectron repulsion, $U(i,j)$ and spin–orbit coupling, $\mathbf{l}\cdot\mathbf{s}$, acting on a basis set derived from the multiplet states arising from an 'atom-like' d^n configuration. The two-electron inter-electron repulsion term and the relativistic spin–orbit coupling term can thus be handled within the central field – *i.e.* spherical – approximation used for isolated atoms and ions. The molecular symmetry is only incorporated into the one-electron, ligand field potential, V_{LF}, and the M–L bonding interactions are captured implicitly in the sequence and energies of the d orbitals.

This form of LFT is thus a many-electron, relativistic treatment capable of making direct contact with experimental observables which are inherently many-electron quantities. It is thus quite different from the simple (and simplistic) qualitative molecular orbital (MO) picture often touted as ligand field theory. In this work, the label 'LFT' will not be applied to this MO version.

$$\mathscr{h}_{\mathrm{LF}} = \sum_{i<j}^{N_{\mathrm{d}}} U(i,j) + \sum_{i}^{N_{\mathrm{d}}} V_{\mathrm{LF}}(\mathbf{r}_i) + \zeta \sum_{i}^{N_{\mathrm{d}}} \mathbf{l}_i \cdot \mathbf{s}_i \qquad (4)$$

2.2. *Ab initio* LFT

The aiLFT method[15–18] is a correlated, multireference wavefunction method which encapsulates the central features of LFT but, in contrast to the parametric formulation, aiLFT is completely independent of experiment. It involves a complete active space self consistent field (CASSCF) calculation where the active space comprises the five mainly-d molecular orbitals (*i.e.* those with a total Löwdin d component greater than 50%) containing the n electrons of the formal d^n metal configuration. The CASSCF treatment of static electron correlation is then augmented by an n-electron valence state perturbation theory (NEVPT2) treatment of dynamic correlation. The aiLFT approach generates the same number of states as that from the d^n configuration and the wavefunction results can be directly mapped onto an equivalent LFT description. A fitting procedure then extracts the underlying ligand field d orbital energies and Racah interelectron repulsion parameter values of the aiLFT Hamiltonian. Subsequent fitting of the aiLFT d orbital energies using a conventional AOM/CLF analysis affords e_λ parameter values which can be used to interpret the local M–L chemical bonding.

For example, the d^2 configuration is 45-fold degenerate and, within the Russell–Saunders coupling scheme, generates five many-electron terms, ^{3}F, ^{3}P, ^{1}S, ^{1}D and ^{1}G which are 21, 9, 1, 5 and 9-fold degenerate respectively. The energies of these 'free ion' terms can be expressed in terms of electrostatic d–d interelectron repulsion parameters either using the original Condon–Shortley scheme (F_0, F_2 and F_4) or the Racah scheme (A, B and C) (see ESI†). In the presence of a ligand field, the terms split. The term energies now have an additional dependence on the d-orbital separations. Thus, there are 10 spin triplets and 15 spin singlets for the state averaged CASSCF procedure to compute. The aiLFT procedure then determines the values of the Racah parameters and d orbital energies which deliver the best fit to the CASSCF results. The choice of active space and number of states guarantees that the active orbital populations for a given d^n system are $n/5$ which maps on to the ligand field idea of an atom-like d configuration arising from the presumed dominant spherical contribution to the ligand field.

All the calculations employed the ORCA program system,[19,20] version 4.2.1. All molecules were initially geometry-optimised using the BP86 functional with def2-SVP basis sets for all atoms bar the metal centre where a def2-TZVP basis is used. Grimme empirical dispersion corrections (keyword D3BJ) and a CPCM solvation field appropriate to ethanol or water were included. For paramagnetic systems, a spin-unrestricted approach was used.

Cartesian coordinates for all the systems considered here and further details of the aiLFT protocol are included in the ESI.†

3. Results and discussion

An important characteristic of the ligand field approach, both parametric and *ab initio*, is the separation of the one-electron and two-electron contributions. The former generate a set of orbitals which provides a powerful insight into the nature of metal–ligand bonding. The developers of aiLFT demonstrated that it is able to 'recover the ligand field picture from ai data' and with an accuracy comparable to the conventional parametric approach.[15] While neither framework is perfect, there are many useful empirical trends derived from parametric ligand field analysis and aiLFT appears to reproduce them faithfully. We will rely on this qualitative correspondence here and base our analysis exclusively on aiLFT results.

3.1. Planar $[Cu(CF_3)_4]^-$ and related systems

$[Cu(CF_3)_4]^-$ has attracted a lot of experimental and theoretical interest, much of it centred on the formal oxidation state and d configuration of the metal centre.[12–14,21–25] At first sight, this complex is a low-spin d^8 Cu^{III} system which is consistent with the nearly planar structure (Fig. 5, top). The slight D_{2d} distortion (the large C–Cu–C angle is 168°) is due to steric interactions between the F atoms. Smaller CH_3 ligands generate basically the same ligand field (*vide infra*) as CF_3 but the geometry is now strictly planar (Fig. 5, middle). In contrast, an unambiguously d^{10} system such as the model compound $[Zn(CF_3)_4]^{2-}$ is tetrahedral (Fig. 5, bottom).

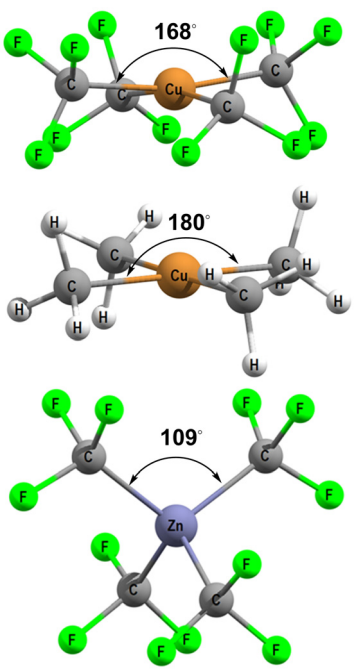

Fig. 5 DFT-optimised structures for $[Cu(CF_3)_4]^-$ (top), $[Cu(CH_3)_4]^-$ (middle) and $[Zn(CF_3)_4]^{2-}$ (bottom).

Of special interest here is the suggestion of a so-called 'inverted ligand field' for $[Cu(CF_3)_4]^-$.[12,13] As described in the introduction, an inverted ligand field is a feature of the MO model. For $[Cu(CF_3)_4]^-$, the inversion results in the (mostly) σ-type d orbital (d_{xy} in D_{2d} symmetry) becoming bonding and thus filled. Compared to the Cu(III) d^8 formulation, this inversion can be interpreted as tantamount to a two-electron reduction of the metal centre. However, this mechanism relies on the overlap between metal-centred and ligand-centred functions which is not possible in the d-orbital-only formulation of LFT.

The only explicit orbitals in LFT are the metal d functions and the d-orbital sequence can never be inverted simply by increasing the σ-bonding covalency. However, if there really is an internal electron transfer, the initially-assumed d configuration should no longer apply and the aiLFT calculation would be expected to fail.

The results of the aiLFT calculations for $[Cu(CF_3)_4]^-$ and $[Cu(CH_3)_4]^-$ are presented in Table 1. The active space orbitals are dominated by d contributions of 61% or more, the d orbital splitting is the 1 : 4 pattern typical of planar complexes with the σ-bonding d_{xy} much higher than the other four, and the Racah parameters are reasonable given that aiLFT tends to overestimate their magnitudes compared to empirical values obtained by fitting experimental d–d spectra.[15,17] Overall, therefore, aiLFT supports the low-spin d^8 Cu^{III} formulation.

The CLF bonding parameters for $[Cu(CF_3)_4]^-$, and a series of related complexes, were derived by fitting the aiLFT d orbital energies and are given in Table 2.[26] These planar, or near planar, systems include contributions from the 'coordination voids' above and below the plane of the molecule as required by the CLF model.[27–29] For the cyanide complexes, there are four parameters but only three degrees of freedom in D_{4h} symmetry so the nominal values of e_π(void) have been chosen to correlate roughly with the magnitude of e_σ(void). Both $[CF_3]^-$ and $[CH_3]^-$ are assumed to be σ-bonding-only although the author acknowledges that there is evidence that the aiLFT introduces a small π-bonding contribution in related M–NH_3 interactions[30] which, if repeated for alkyl ligands, would directly influence the e_π(void) parameter. However, the magnitudes of the $e_\pi(NH_3)$ parameters is of the order of 500 to 1000 cm^{-1} which would not be significant here.

Comparing the Cu^{III} species at the CAS level, $e_\sigma(L_{eq})$ is ~12 000 ± 250 cm^{-1}, e_σ(void) is −8000 ± 1000 cm^{-1} and

Table 1 aiLFT results for $[Cu(CF_3)_4]^-$ and $[Cu(CH_3)_4]^-$. %d refers to the Lowdin percentage contribution of the appropriate d orbital in the active space. All relative d orbitals energies and Racah *B* and *C* parameters are in cm^{-1}

	$[Cu(CF_3)_4]^-$			$[Cu(CH_3)_4]^-$		
aiLFT data	%d	Δ*E*(CAS)	Δ*E*(NEVPT2)	%d	Δ*E*(CAS)	Δ*E*(NEVPT2)
d_{xy}	61	38 617	65 898	58	40 830	72 024
$d_{x^2-y^2}$	99	1985	0	98	3954	3033
d_{z^2}	91	1121	1564	93	211	1481
d_{xz}	93	2	1037	98	0	0
d_{yz}	93	0	1032	98	0	0
B	—	1018	1249	—	1068	1262
C	—	5297	2962	—	5506	3012

Table 2 AOM/CLF parameter values derived from fitting the aiLFT CASSCF active space orbital energies

Complex	Symmetry	Level	e_σ(eq)	e_π(eq)	e_σ(void)	e_π(void)
$[Cu^{III}(CF_3)_4]^-$	D_{2d}	CAS	12 500	0[a]	−7000	−1400
		NEVPT2	22 450	0[a]	−9900	−200
$[Cu^{III}(CH_3)_4]^-$	D_{4h}	CAS	12 300	0[a]	−8150	−1980
		NEVPT2	22 997	0[a]	−12 239	−1516
$[Ni^{II}(CF_3)_4]^{2-}$	D_{2d}	CAS	7200	0[a]	−4700	−1100
$[Ni^{II}(CN)_4]^{2-}$	D_{4h}	CAS	8400	−400	−5850	*−1200*[a]
$[Cu^{III}(CN)_4]^-$	D_{4h}	CAS	11 900	−400	−9000	*−2000*[a]

[a] Assumed value.

e_π(void) is $\sim -1700 \pm 300$ cm^{-1}. Thus, from an *ab initio* ligand field perspective, $[CF_3]^-$, $[CH_3]^-$ and $[CN]^-$ generate similar, strong ligand fields, implying strong metal–ligand covalency, but that there is little distinction between a cyanide 'coordination complex' and a methyl or trifluoromethyl 'organometallic compound'.

The aiLFT results support a d^8 Cu(III) formulation while the MO approach is more consistent with d^{10} Cu(I). However, both conclusions depend on the orbitals of the model and the aiLFT d orbitals are very different from the orbitals of MO theory. It should therefore come as no surprise that the two frameworks give different 'answers' which, at first sight, may appear to be at odds. Leach *et al.*[22] attempt to bridge the two extremes by proposing a quasi-d^{10} formulation which allows for the effects of covalency to alter the actual d orbital populations while Alayoglu *et al.*[21] propose further experimental support for the Cu(I) formulation. However, irrespective of the mechanisms permitted by our choices of model, whether theoretical[12,22,31] or experimental, at the very least we can all agree that the Cu–C bonds in $[Cu(CF_3)_4]^-$ are very covalent.

3.2. $[M(CO)_6]^m$

The octahedral metal carbonyl compounds $[Fe(CO)_6]^{2+}$, $[Mn(CO)_6]^+$, $Cr(CO)_6$, $[V(CO)_6]^-$ and $[Ti(CO)_6]^{2-}$ provide a further test of how much the ligand field regime overlaps what is conventionally considered as organometallic chemistry. The calculated results are given in see Table 3.

All five species are formally 18-electron, low-spin d^6 compounds. However, only $[Fe(CO)_6]^{2+}$, $[Mn(CO)_6]^+$ and $Cr(CO)_6$ maintain the integrity of the d-orbital active space: $[V(CO)_6]^-$ has one of the e_g orbitals replaced by a mainly metal-s orbital while for $[Ti(CO)_6]^{2-}$, both metal e_g orbitals have been swapped out for ligand-based functions.

Thus, the aiLFT protocol developed here has limits. Given that there is a smooth progression in the experimental C–O stretching mode energy from 2204 cm^{-1} for $[Fe(CO)_6]^{2+}$ through to 1750 cm^{-1} for $[Ti(CO)_6]^{2-}$, this seems to be more an issue with aiLFT rather than any fundamental change in the nature of the bonding. Nevertheless, any derived parameters from 'failed' aiLFT calculations need to be treated with extreme caution.

Table 3 DFT geometries and aiLFT results for hexacarbonyl compounds. Bond lengths in Å and energies in cm^{-1}

Compound	r(M–C)	R(C–O)	%d(t_{2g})	%d(e_g)	Δ_{oct}(CAS)	Δ_{oct}(NEVPT2)
$[Fe(CO)_6]^{2+}$	1.876	1.134	94.4	85.4	30 750	37 900
$[Mn(CO)_6]^+$	1.878	1.145	83.5	85.2	35 670	48 090
$Cr(CO)_6$	1.900	1.153	67.7	83.9	42 000	60 660
$[V(CO)_6]^-$	1.954	1.173	*60–65*	*	*	*
$[Ti(CO)_6]^{2-}$	2.043	1.189	*51–58*	*	*	*

For $[Fe(CO)_6]^{2+}$, $[Mn(CO)_6]^+$ and $Cr(CO)_6$ where the aiLFT protocol gives acceptable results, separate e_σ and e_π parameters can be extracted by applying a small trigonal elongation of $\sim 3^\circ$ which splits the nominal t_{2g} dπ orbitals (Fig. 6, left). The sense of the dπ orbital splitting, ΔE_1, determines sign of e_π (Fig. 6, right).

The ligand field bonding picture (see Table 4) has carbonyl acting as a good σ donor and progressively stronger π acceptor for Fe to Cr. There is a suggestion that π acceptance saturates as the metal oxidation state approaches zero although the estimate of e_π is very sensitive to the ΔE_1 value. The ligand field bonding picture in these metal carbonyl species, derived exclusively from considering just the d orbitals, is thus in agreement with conclusions based on MO treatments.[32]

3.3. Metallocenes and η^n-bonded ligands

Metallocenes are the 'poster children' for organometallic chemistry but are nevertheless generally well-treated by LFT.[33] Historically, this relied on the correct identification of experimental spectroscopic data which, even for the archetype ferrocene, is an issue.[34] However, given reliable data, the electronic structures of metallocenes are well-reproduced by ligand field calculations. However, as for the octahedral $M(CO)_6$ systems mentioned above, the high symmetry makes the CLF analysis of the bonding picture ambiguous.

In LFT, $M(Cp)_2$ compounds are modelled as linear ML_2 systems with effective $D_{\infty h}/C_{\infty v}$ symmetry. The d orbitals split into a 1 : 2 : 2 pattern with a clean symmetry separation of $d\sigma(d_{z^2}) : d\pi(d_{xz}/d_{yz}) : d\delta(d_{xy}/d_{x^2-y^2})$. There are two degrees of freedom in this model. However, the Cp^- ligand has six valence electrons in five π-type orbitals and, with respect to the Cp–M interaction, there are one σ donor, two π donor and two δ acceptor orbitals (Fig. 7). This requires three CLF parameters: e_σ and e_π which should be positive and e_δ which should be negative.

The geometry of metallocenes, and indeed other homoleptic sandwich compounds, places the ligand bonding electron

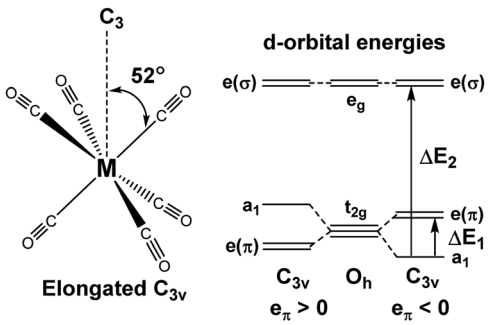

Fig. 6 Trigonal distortion applied to $M(CO)_6$ compounds and relationship between the sense of splitting of the t_{2g} orbitals and the sign of the e_π parameter.

Table 4 AOM parameters derived from aiLFT calculations on C_{3v} symmetry $M(CO)_6$ systems

Compound	CAS ΔE_1	CAS ΔE_2	CAS $e_\sigma(CO)^a$	CAS $e_\pi(CO)^a$	NEVPT2 ΔE_1	NEVPT2 ΔE_2	NEVPT2 $e_\sigma(CO)^a$	NEVPT2 $e_\pi(CO)^a$
$[Fe(CO)_6]^{2+}$	650	31 700	7700	−2200	990	39 950	9200	−3100
$[Mn(CO)_6]^{+}$	1770	42 080	7300	−5100	2972	53 775	7100	−8100
$Cr(CO)_6$	1758	52 350	10 800	−5000	3327	61 767	8500	−9000

[a] To nearest 100 cm^{-1}.

density close to the nodal surface of the metal d_{z^2} orbital. Hence, the σ interaction is expected to be relatively minor and e_σ should be small. In contrast, M–L π bonding is strong and e_π should be large and positive. The significance of M–L δ-backbonding varies with the ligand.

The ligand field analysis for a general, linear $M(\eta^n\text{-L})_2$ system (Fig. 8) gives $e_\sigma - e_\delta = \frac{1}{2}[\Delta E(z^2)]$ where $\Delta E(z^2) = E(d_{z^2}) - E(d_{xy})$. For $Fe(Cp)_2$, aiLFT gives $\Delta E(z^2)$ at ~3000 cm^{-1} at the CASSCF level (Table 5). Thus, if σ-bonding is presumed to be minor – $e_\sigma(Cp)$ is, say, ~500 to 1000 cm^{-1} – then so too is the Fe–Cp δ interaction ($e_\delta \sim -1000$ to -500 cm^{-1}) and the Fe–Cp π bond is dominant ($e_\pi \sim 10\,000$ cm^{-1}). It should be noted that the sense of the $d_{z^2}/(d_{x^2-y^2},d_{xy})$ splitting determines whether the Cp^- ligand is a δ-donor ($d_{z^2} < d_{x^2-y^2}/d_{xy}$) or a δ-acceptor (Fig. 9). Canonical DFT orbitals give a 'ligand field' with d_{z^2} lower than $d_{x^2-y^2}/d_{xy}$ thus suggesting Cp^- is a δ-donor.[34] In contrast, the CLF analysis, the empty acceptor δ orbitals on the Cp^- pro-ligand, the filled δ donor orbitals on the Fe centre and a DFT-based energy decomposition analysis (EDA) (*vide infra*) all support Cp^- being a δ-acceptor.[35] Great care should be taken in interpreting the relationship between canonical orbitals and the nature of M–L bonding.[36]

There is no ambiguity for $Cr(C_6H_6)_2$. Both canonical DFT and aiLFT place d_{z^2} substantially above the dδ orbitals and benzene is thus a much stronger δ acceptor than Cp^-. The aiLFT energy difference $\Delta E(z^2)$ in $Cr(C_6H_6)_2$ is ~20 000 cm^{-1} so that if e_σ is still presumed to relatively small, $e_\delta(C_6H_6)$ is substantial (~−10 000 cm^{-1}) with e_π being of comparable magnitude, although the latter varies quite steeply as a function of e_σ. Qualitatively, therefore, ligand field analysis of the aiLFT d orbital energies suggests that the Cp^- ligands in $Fe(Cp)_2$ are strong π donors, but relatively weak σ donors and weak δ acceptors, while the C_6H_6 ligands in $Cr(C_6H_6)_2$ are weak σ donors but strong π donors and strong δ acceptors. In both cases, the dπ orbitals are the most destabilised.

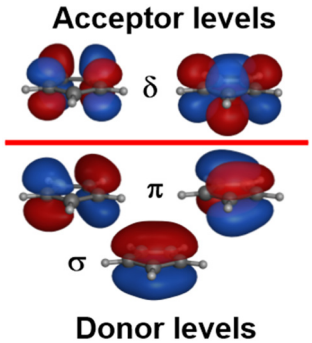

Fig. 7 Schematic MO plots of valence π orbitals for Cp^-.

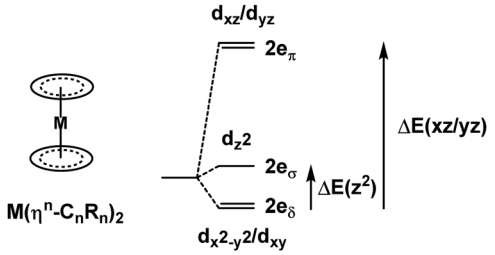

Fig. 8 Generic AOM/CLF energy level diagram for sandwich compounds.

Table 5 CLF parameters derived from CASSCF aiLFT results for $Fe(Cp)_2$ and $Cr(C_6H_6)_2$

Compound	$Fe(Cp)_2$		$Cr(C_6H_6)_2$	
$\Delta E(z^2)^a$	2777		20 137	
$\Delta E(xz/yz)^a$	21 686		36 277/39 870	
e_σ	0	1389	0	10 068
e_π	9455	10 843	8070	18 138
e_δ	−1389	0	−10 068	0

[a] Energies in cm^{-1} relative to d_{xy} and $d_{x^2-y^2}$.

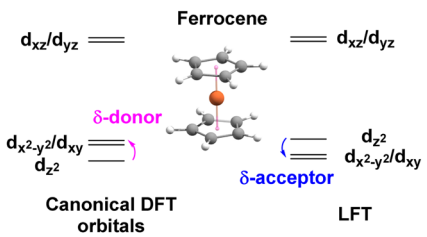

Fig. 9 Ferrocene d-orbital splitting diagrams.

This ligand field picture compares quite well to the DFT-based EDA analysis of Rayon and Frenking.[35] They too conclude that $Fe(Cp)_2$ is dominated by Fe–Cp π bonding but suggest that δ dominates π bonding in $Cr(C_6H_6)_2$. The ligand field picture has much more equal π and δ contributions. The difference can probably be attributed to the metal reference states.

The ligand field reference state is spherically symmetric and the d orbitals are equally occupied: 1.2 per orbital for d^6 systems. The state averaged CASSCF of aiLFT gives the same result. In contrast, the EDA analysis used a 'prepared' Cr atom with a $d_z2^2 d_{xy}{}^2 d_{x^2-y^2}{}^2$ configuration. Thus, the EDA analysis starts with four electrons in the metal δ orbitals while the

LFT/aiLFT δ population for a d^6 system is only 2.4 consistent with the EDA calculation favouring δ backbonding more than LFT. Nevertheless, it is encouraging to note that the bonding pictures derived from two quite different approaches, are broadly the same.

3.4. $[Ni(Cp)_2]^{2+}$: the aiLFT protocol fails

The recently-reported $[Ni(Cp)_2]^{2+}$ species provides further insights into the aiLFT protocol in particular and LFT in general. Formally, this is a d^6 Ni(IV) compound which is the highest reported oxidation state for Ni.[37] However, higher oxidation states require hard, electronegative donors like F^- so strongly covalent ligands like Cp^- should not be able to support a formal +4 charge on the metal centre. The authors go further and suggest, based on an atoms-in-molecule atomic charge analysis, that the actual metal charges in $[Ni^{II}(Cp)_2]$, $[Ni^{III}(Cp)_2]^+$ and $[Ni^{IV}(Cp)_2]^{2+}$ are all about the same and that it is the Cp ligand charge which varies with the total charge.[38]

If this is true, then the aiLFT assumption of a d^6 configuration for $[Ni(Cp)_2]^{2+}$ should not be valid. In agreement with this suggestion, the aiLFT calculation fails (Table 6). This result is not an artefact, since aiLFT calculations for 20-electron, high-spin d^8 $[Ni^{II}(Cp)_2]$ and 18-electron, low-spin d^6 $[Ni^{IV}F_6]^{2-}$ maintain the integrity of the presumed d configuration (Table 6). This behaviour simply reflects that there are ligand- and geometry-dependent limits on the maximum formal oxidation state the metal can achieve. This is a well-known phenomenon illustrated, for example, by the so-called 'oxo-wall' for tetragonal first-row metal-oxo complexes.[39]

3.5. Pauli shields and the ligand field and ultra-covalent regimes

The numerical success of ligand field theory is due to the special nature of the 'inner' $(n-1)$d orbitals which are shielded from strong covalent overlap with ligand orbitals by the Pauli repulsion arising from the semi-core, $(n-1)$s and $(n-1)$p metal orbitals (Fig. 10).[40,41] This is particularly marked for 3d systems where the valence d orbitals have no radial node. The 3s and 3p orbitals are of comparable size to the 3d, but completely filled, which generates a 'Pauli shield' that leads to 'stretched' metal–ligand bonds. The ligand-field d orbitals are thus 'atom-like' and the central-field approximations used for d–d inter-electron repulsion and spin–orbit coupling are reasonably accurate. Systems where the Pauli shield ensures the integrity of the d^n configuration are deemed to be in the 'ligand field regime' as depicted in Fig. 11, left.

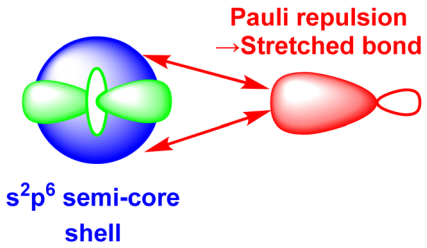

Fig. 10 Schematic representation of the origins of the 'Pauli shield'. (After Fig. 3 of ref. 41.) The $(n-1)$s, $(n-1)$p and $(n-1)$d orbitals on the metal have comparable radii and the red double-headed arrows indicate the Pauli repulsion from the electrons in the filled s and p semi-core orbitals on the electron pair in the ligand σ bond (red).

The ligand field analyses presented above suggest two mechanisms by which this Pauli shield might be breached. The $M(CO)_6$ series conjures a picture of the metal being 'overwhelmed' as its formal oxidation state becomes more and more negative. The metal becomes so electron rich, and the π back-donation so strong, that metal d electrons overcome the Pauli shield from the 'inside' and 'flood' out into the ligand region as depicted schematically in Fig. 11, top right. Alternatively, and as exemplified by the behaviour of $[Ni(Cp)_2]^{2+}$, when the metal oxidation state becomes too positive, the d orbitals are dragged down so far that the Pauli shield is breached from the 'outside' and any empty metal d orbitals become filled by bonding electron density (Fig. 11, bottom right). This internal electron transfer is basically the same mechanism as the inverted ligand field of MO theory. In either event, the extreme 'ultra-covalency' destroys the integrity of the assumed aiLFT d configuration as well as the formal oxidation state.

Evidence for an imminent Pauli shield breach from the inside can be found in the aiLFT calculations for the metal hexacarbonyl series. The t_{2g}/e_g percentage compositions of the active orbitals for $[Fe^{II}(CO)_6]^{2+}$, $[Mn^{I}(CO)_6]^+$ and $Cr^0(CO)_6$ are 94/85, 84/85 and 66/84 respectively. The d component of the t_{2g} orbitals drops progressively while the composition of the σ-type e_g orbitals remains virtually constant. This correlates with only the t_{2g} orbitals being occupied and hence solely responsible for any 'internal' Pauli shield breach. We should note also that at 61%, the d_{xy} component of the Cu–C σ orbital in the active space of $[Cu(CF_3)_4]^-$ also suggests a system close to a Pauli shield breach.

Table 6 aiLFT results for nickel compounds. All energies in cm^{-1}

	$Ni(Cp)_2$			$[Ni(Cp)_2]^{2+}$			$[NiF_6]^{2-}$		
aiLFT data	%d	Δ*E*(CAS)	Δ*E*(NEVPT2)	%d	Δ*E*(CAS)	Δ*E*(NEVPT2)	%d	Δ*E*(CAS)[a]	Δ*E*(NEVPT2)[a]
d_{xy}	99	0	0	8	1347	1321	90	3	20
$d_{x^2-y^2}$	99	0	0	89	7588	85 186	67	20 857	28 128
d_{z^2}	98	1244	1037	95	0	0	67	20 852	28 100
d_{xz}	88	11 372	17 541	28	33453	92 062	90	0	0
d_{yz}	88	11 372	17 541	33	30 356	90 454	90	1	15
B	—	1195	1136	—	−937	1261	—	977	1083
C	—	4448	3727	—	10 634	−9883	—	4561	2789

[a] Minor deviations from rigorous O_h symmetry due to small amount of 'noise' from the solvent field.

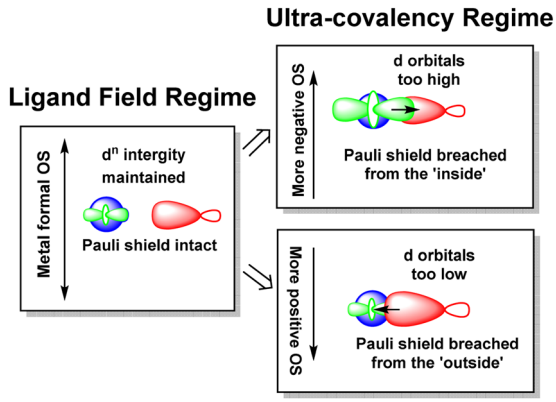

Fig. 11 Schematic depiction of the ligand field regime, where the d^n integrity is maintained, and the two scenarios in which this integrity is lost and the Pauli shield is breached.

The sandwich compounds illustrate a number of interesting features culminating in a Pauli shield breach from the outside for $[Ni(Cp)_2]^{2+}$ (Fig. 12). In common with octahedral V^{II} complexes, $V(Cp)_2$ has three low-energy d orbitals of similar energies and is therefore a high spin d^3 system although the overall d orbital splitting is larger than the spin-pairing energy. The ligand field in $Fe(Cp)_2$ is even stronger and with the higher d electron count, multiple spin states are possible with the low-spin d^6 configuration favoured. However, the low-energy d orbitals must be above the bonding level threshold (the red dashed line in Fig. 12) since the oxidised low-spin d^5 ferrocenium cation is paramagnetic but stable: that is, the 'hole' is not immediately swamped by bonding electron density. Ferrocene thus has a lot in common with ferrocyanide.

The total ligand field splitting of $Cr(C_6H_6)_2$ is almost twice that of $Fe(Cp)_2$ which could mean that the lower d orbitals on chromium lie below the bonding threshold as depicted in Fig. 12. However, since they are already full, there are no internal electron transfer consequences. On the other hand, the strong stereochemical activity of the electrons in the strongly anti-bonding dπ orbitals of high-spin d^8 $Ni(Cp)_2$ lengthens the Ni–C distances by about 0.2 Å compared to the Fe–C distances in ferrocene and reduces the total ligand field splitting by about half. $Ni(Cp)_2$ is therefore a weak field compound, the d^8 configuration is well protected by the Pauli shield and the d orbitals are above the bonding threshold. However, the removal of the two dπ electrons to generate $[Ni(Cp)_2]^{2+}$ results in a dramatic shortening of the Ni–C distances and a sharp increase in Ni–Cp covalency which has a catastrophic effect on the d orbital energies. These descend well below the bonding threshold, the Pauli shield is breached from the outside, and the d^6 configuration loses its integrity.

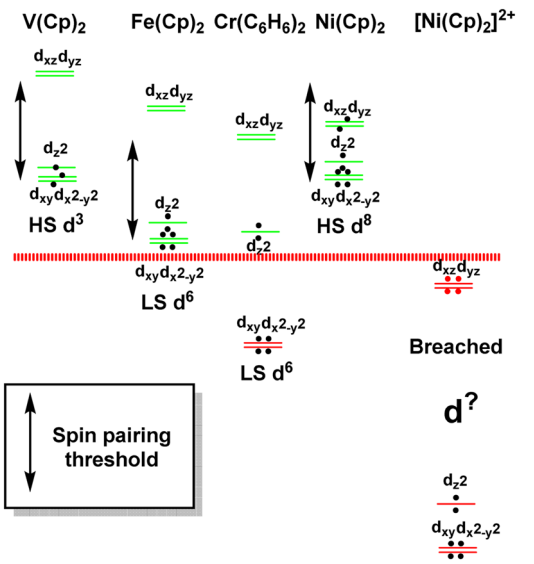

Fig. 12 Schematic representation of the d orbital energies relative to the bonding level threshold (red dotted line) for a selection of organometallic sandwich compounds.

Clearly, the aiLFT calculations correlate strongly with both the strength of ligand field and the formal metal oxidation state. Using the compounds already analysed and some additional species, the limits of this *ab initio* ligand field envelope are displayed in Fig. 13. Significantly, within the bounds of where the ligand field/metal oxidation state combinations retain the d configuration integrity, the *ab initio* ligand field picture applies equally to 'ionic' Werner-type coordination complexes species and 'covalent' organometallic compounds. Hence, for all these systems, the same conceptual picture applies and the nature of the metal–ligand bonding can be inferred by analysing just the ligand field d orbitals.

3.6. The ligand field picture and valence electron counts

The ligand field picture involves the projection of the M–L bonding interactions onto the metal d orbitals and thus, the d orbitals are the only explicit functions we need to consider. The bonding electrons are implicit in the CLF parameters. Each positive e_λ parameter represents an individual ligand–metal donor interaction of λ symmetry and involves a pair of electrons.

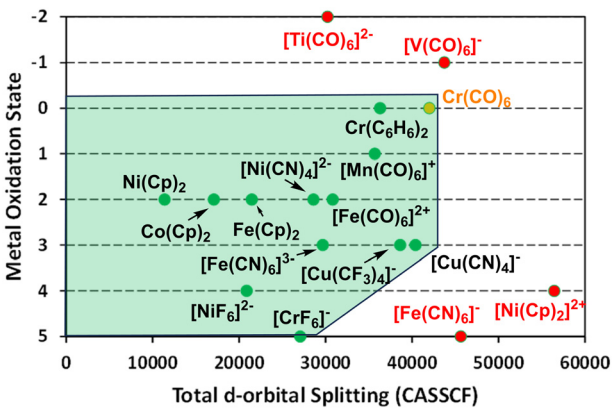

Fig. 13 Schematic representation of the ligand field regime envelope (green shading). Compounds are ordered by formal metal oxidation state and the maximum d-orbital separation at the aiLFT CASSCF level. Green dots indicate the integrity of the d^n configuration is maintained; orange that the configuration is near the breaching limit and red, that the Pauli shield has been breached and the d^n integrity has been destroyed. Their d-orbital splitting energies are thus approximate only.

Negative e_λ parameters represent individual ligand–metal acceptor interactions of λ symmetry which affect the relevant d orbital energies but make no contribution to the valence electron count. For example, a CO ligand has a positive e_σ and a negative e_π and is a two-electron donor while Cp^- and C_6H_6 have a positive e_σ, a positive e_π (*i.e.* $e_{\pi x} = e_{\pi y}$) and a negative e_δ (*i.e.* $e_{\delta xy} = e_{\delta x^2-y^2}$) and are six-electron donors. (F^- is formally an 8-electron donor but this issue will be dealt with in a future publication.)

The electron count on the metal depends on its formal oxidation state. All the electrons are placed in its d orbitals. Thus, the CLF scheme for $Cr(CO)_6$ comprises six positive $e_\sigma(CO)$ and six negative $e_\pi(CO)$ giving 12 bonding electrons plus six electrons from the Cr^0 centre: 18-electrons in total.

To account for the ligand field analyses discussed above, a Pauli shield was invoked to 'protect' the d orbitals from the bonding electrons. If the d orbitals get too low, as can occur for strongly-covalent and ultra-covalent systems, the Pauli shield can be breached. However, if these low-energy d orbitals are already filled, internal electron transfer is prevented and there are no significant consequences. The optimal d-electron counts thus correspond to filling up any low-lying d orbitals.

The binary metal carbonyls provide an good illustration and the CLF d-orbital energy level diagrams for four-, five- and six-coordinate compounds are shown schematically in Fig. 14 assuming $e_\pi = -1/2e_\sigma$ for illustrative purposes. For each symmetry, the σ-only bonding pattern is on the left and this connects to the pattern on the right which includes the effects of M–L π acceptance and the depression of the d_{z^2} orbital in square pyramidal and square planar symmetry due to d–s mixing.[42–44]

Fig. 14 emphasises that the key feature is the number of strongly destabilised d orbitals which are above the bonding threshold. For a threshold energy equivalent to about $2e_\sigma$, tetrahedral symmetry has no high-energy d orbitals, trigonal bipyramidal, square pyramidal and square planar compounds have one and octahedral symmetry has two. The optimal d electron counts are respectively 10, 8, 8, 8 and 6, and the bonding electron counts are 8, 10, 10, 8 and 12 giving total valence electron counts of 18, 18, 18, 16 and 18.

Note that these electron counts and, by association, the '18-electron rule', depend on the magnitude of the ligand field. As shown in Fig. 9, for $Fe(Cp)_2$ there are three low-energy d orbitals and an electron count of 18 but since the ligand field from Cp^- is relatively weak, this is fortuitous. Neutral metallocenes behave like other coordination complexes of divalent metals and can support multiple electron counts. For example, vanadocene, like $[V(OH_2)_6]^{2+}$, is only a 15-electron species while nickelocene, like $[Ni(NH_3)_6]^{2+}$ is a 20-electron species. Moreover, the 17 electron ferrocenium cation is perfectly stable. If the ligand field is sufficiently low that the Pauli shield remains intact, the 18-electron rule need not apply.

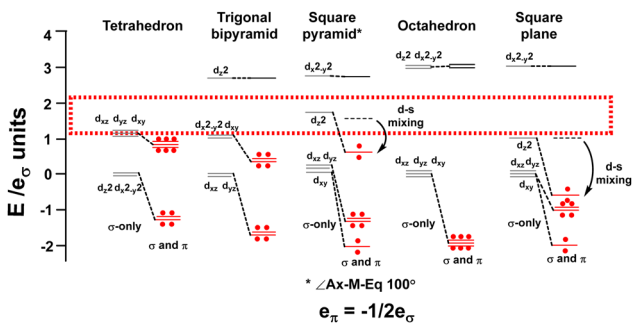

Fig. 14 Optimal metal d electron counts (red dots) relate to d orbital splittings for strongly covalent $M(CO)_6$ systems where the bonding threshold (dotted rectangle) is high.

3.7. Transition metal chemistry: κ- and η-bonded ligands

An important aspect of this work is the identification, in ligand field terms, of the M–L bonding features common to transition metal compounds. On the one hand, there are compounds where the ligands are κ-type and the σ-donor interaction is usually dominant ($e_\sigma \gg e_\pi$). This covers all of coordination chemistry and a significant number of organometallic compounds. On the other hand, there are the η^n-type systems where π-donation is usually dominant ($e_\pi \gg e_\sigma$). For cyclic η^n ligands, where $n > 3$, there is also the possibility of additional δ interactions. Haptic bonding is the exclusive domain of organometallic chemistry yet, significantly, the ligand field picture applies equally well to ferrocene as it does to ferrocyanide. This relatively simple conceptual framework thus puts all transition metal molecules on the same footing.

4. Conclusions

The ligand field bonding picture formulated by Gerloch and Woolley treats the metal–ligand interactions implicitly *via* local σ, π and δ parameters. Their various effects are then reflected in the sequence and energy separations of the ligand field d orbitals. These are the only explicit orbitals in the model.

Ligand-field analysis is well established in coordination chemistry and many features of metal complexes can be rationalised based solely on the metal d orbitals. However, the dearth of suitable 'ligand-field' experimental data for organometallic compounds makes it difficult, or impossible, to assess whether the ligand field picture even applies. In this paper, *ab initio* LFT has been employed as an experimental surrogate to explore the ligand field envelope computationally to try and establish the extent of the ligand field regime.

Calculated aiLFT d-orbital energies have been analysed within the CLF framework. Three types of compound have been considered: (i) the formally low-spin d^8 complex $[Cu^{III}(CF_3)_4]^-$; (ii) the low-spin d^6 hexacarbonyls $[Fe^{II}(CO)_6]^{2+}$, $[Mn^{I}(CO)_6]^+$, $[Cr^0(CO)_6]$, $[V^{-I}(CO)_6]^-$ and $[Ti^{-II}(CO)_6]^{2-}$; and (iii) the sandwich compounds d^6 $[Fe^{II}(Cp)_2]$, d^8 $[Ni^{II}(Cp)_2]$, d^6 $[Ni^{IV}(Cp)_2]^{2+}$ and d^6 $Cr(C_6H_6)_2$. The first two groups are κ-bonded systems requiring only σ and π bonding parameters with σ-donor interactions dominant. The η^n-bonded cyclic ligands have significant M–L π-donor bonding with an additional δ-acceptor component.

The aiLFT protocol shows that the ligand fields of CO, Cp^-, C_6H_6, $[CF_3]^-$ and $[CH_3]^-$ are comparable to that of cyanide and the formal oxidation states and d configurations for most of the complexes of these ligands are retained. Ligand field analyses of the aiLFT d orbital energies suggest that CO is a strong σ donor and, as the metal oxidation state becomes less positive, a progressively stronger π acceptor. Cp^- is a good π donor, a weak σ donor and a relatively poor δ acceptor. C_6H_6 is also a good π donor and weak σ donor but is a much better δ acceptor than Cp^-. Thus, both organometallic and coordination compounds falls within the *ab initio* ligand field envelope. However, there are limits on the oxidation state/ligand combination and the aiLFT protocol fails for $[V(CO)_6]^-$, $[Ti(CO)_6]^{2-}$ and $[Ni(Cp)_2]^{2+}$.

For $[V(CO)_6]^-$ and $[Ti(CO)_6]^{2-}$ the oxidation state is too negative and the $3s^23p^6$ 'Pauli shield' is breached from the inside. For $[Ni(Cp)_2]^{2+}$, the oxidation state is too positive and the aiLFT protocol fails because the Pauli shield is breached from the outside.

A visual representation of the boundary between the ligand field regime and the ultra-covalent regime is based on the total aiLFT d orbital splitting and the formal metal oxidation state. For M^0 to M^{III}, the CASSCF limit is about 42 000 cm^{-1} and all the ligands considered here give complexes within the ligand field envelope (Fig. 13). This includes $[Cu(CF_3)_4]^-$ which, according to the aiLFT protocol developed here, should be formulated as a low-spin d^8 Cu^{III} species rather than a d^{10} Cu^I compound as suggested by invoking the MO concept of 'inverted ligand fields'. In the d-orbital-only form of LFT, the ligand field can never 'invert' simply by increasing the σ bonding but, crucially, all methods, both theoretical and experimental, agree that the Cu–C bond is very covalent. How this covalency manifests is model dependent.

For the higher oxidation states M^{IV} and M^V, the Pauli threshold is progressively lowered and, as illustrated by $[Ni^{IV}F_6]^{2-}$ and $[Cr^VF_6]^-$, only fluoride is electronegative enough to maintain the integrity of their d configurations. In contrast, the formal oxidation states for $[Ni^{IV}(Cp)_2]^{2+}$ and $[Fe^V(CN)_6]^-$ are too high for the ligand sets and these species lie outside the *ab initio* ligand field envelope. Their presumed d configurations of d^6 and d^3 respectively are not maintained in the aiLFT protocol. This does not necessarily imply that the ligand field picture is failing, rather that the aiLFT methodology can no longer isolate the required d orbitals.

The aiLFT analyses also suggest a simple method for rationalising the electron counts of organometallic compounds. The ligand electron count is based on the CLF parameterisation, which depends on the ligand's electronic structure, while the optimal d-electron count is based on the d orbital splittings. In weak-to-relatively-strong fields, all the d orbitals are above the bonding level threshold and the d electron count can be variable. Thus, Cp^- compounds display electron counts of 15 in $V(Cp)_2$ to 20 in $Ni(Cp)_2$. For stronger-field ligands like CO, only the highest-energy d orbitals are above the bonding threshold and the lower d orbitals are filled. This leads to optimal d-electron counts of 6 for $Cr(CO)_6$, 8 for $Fe(CO)_5$ and 10 for $Ni(CO)_4$ and, since there is only one positive CLF and thus CO is a 2-electron donor, total electron counts of 18. For planar compounds, only $d_{x^2-y^2}$ (assuming D_{4h} symmetry) is above the bonding threshold giving four filled d orbitals and a total valence electron count of 16.

In conclusion, the aiLFT protocol developed here has established that, in addition to the coordination complexes for which it was originally intended, d-orbital-only LFT encompasses a substantial proportion of organometallic chemistry. The main difference is that κ-ligated coordination complexes only require σ and π bonding modes with σ-bonding usually dominant while η^n-ligated systems have dominant π-bonding and are also capable of δ interactions. It is also apparent that d-orbital-only LFT includes important electron correlation effects which simple MO theory does not. In the author's opinion, the LFT label should be reserved for the implicit bonding formalism which, incidentally, has an actual ligand field. This ligand field picture allows the nature of the local M–L σ, π and δ interactions to be extracted simply by analysing the sequence and relative energies of the ligand field d orbitals and the structures and bonding of molecular transition metal systems can be understood using the same conceptual footing. Both coordination and organometallic compounds appear to have much more in common than may have been recognised hitherto.

Data availability

The data supporting this article have been included as part of the ESI.† The code for all the quantum chemical calculations can be found on the ORCA Forum download page **https://orcaforum.kofo.mpg.de/app.php/dlext/**. ORCA version 4.2.1 was employed for this study.

Conflicts of interest

There are no conflicts of interest to declare.

Acknowledgements

There is no funding to report in this work. Thanks to Dr David Fox for many stimulating discussions.

References

1 M. T. Weller, T. I. Overton, J. P. Rourke and F. A. Armstrong, *Inorganic Chemistry*, Oxford University Press, Oxford, 6th edn, 2018.
2 H. A. Bethe, *Ann. Phys.*, 1929, **395**, 133–208.
3 W. H. Kleiner, *J. Chem. Phys.*, 1952, **20**, 1784–1791.
4 J. S. Griffith and L. E. Orgel, *Q. Rev., Chem. Soc.*, 1957, **11**, 381–393.
5 C. J. Ballhausen, *Introduction to Ligand Field Theory*, McGraw-Hill, New York, 1962.
6 M. Gerloch, J. H. Harding and R. G. Woolley, *Struct. Bonding*, 1981, 1–46.

7 M. Gerloch and R. G. Woolley, *J. Chem. Soc., Dalton Trans.*, 1981, 1714–1717.
8 R. G. Woolley, *Mol. Phys.*, 1981, **42**, 703–720.
9 M. Gerloch and R. G. Woolley, *Prog. Inorg. Chem.*, 1983, **31**, 371–446.
10 C. E. Schäffer and C. K. Jorgensen, *Mol. Phys.*, 1965, **9**, 401.
11 R. J. Deeth and M. Gerloch, *J. Chem. Soc., Dalton Trans.*, 1986, 1531–1534.
12 R. Hoffmann, S. Alvarez, C. Mealli, A. Falceto, T. J. Cahill, T. Zeng and G. Manca, *Chem. Rev.*, 2016, **116**, 8173–8192.
13 J. P. Snyder, *Angew. Chem., Int. Ed. Engl.*, 1995, **34**, 80–81.
14 C. Gao, G. Macetti and J. Overgaard, *Inorg. Chem.*, 2019, **58**, 2133–2139.
15 M. Atanasov, D. Ganyushin, K. Sivalingam and F. Neese, in *Molecular Electronic Structures of Transition Metal Complexes II*, ed. D. M. P. Mingos, P. Day and J. P. Dahl, Springer Berlin Heidelberg, Berlin, Heidelberg, 2012, pp. 149–220, DOI: 10.1007/430_2011_57.
16 M. Atanasov, D. Aravena, E. Suturina, E. Bill, D. Maganas and F. Neese, *Coord. Chem. Rev.*, 2015, **289**, 177–214.
17 S. K. Singh, J. Eng, M. Atanasov and F. Neese, *Coord. Chem. Rev.*, 2017, **344**, 2–25.
18 L. Lang, M. Atanasov and F. Neese, *J. Phys. Chem. A*, 2020, **124**, 1025–1037.
19 F. Neese, *Wiley Interdiscip. Rev.: Comput. Mol. Sci.*, 2018, **8**, e1327.
20 F. Neese, *Wiley Interdiscip. Rev.: Comput. Mol. Sci.*, 2012, **2**, 73–78.
21 P. Alayoglu, T. Chang, C. Yan, Y.-S. Chen and N. P. Mankad, *Angew. Chem., Int. Ed.*, 2023, **62**, e202313744.
22 I. F. Leach, R. W. A. Havenith and J. E. M. N. Klein, *Eur. J. Inorg. Chem.*, 2022, e202200247.
23 B. L. Geoghegan, Y. Liu, S. Peredkov, S. Dechert, F. Meyer, S. DeBeer and G. E. Cutsail, *J. Am. Chem. Soc.*, 2022, **144**, 2520–2534.
24 M. Gimferrer, A. Aldossary, P. Salvador and M. Head-Gordon, *J. Chem. Theory Comput.*, 2021, **18**, 309–322.
25 R. C. Walroth, J. T. Lukens, S. N. MacMillan, K. D. Finkelstein and K. M. Lancaster, *J. Am. Chem. Soc.*, 2016, **138**, 1922–1931.
26 The NEVPT2 results give the same trends.
27 R. J. Deeth, *Dalton Trans.*, 2020, **49**, 9641–9650.
28 R. J. Deeth and M. Gerloch, *Inorg. Chem.*, 1984, **23**, 3846–3853.
29 R. J. Deeth, *Eur. J. Inorg. Chem.*, 2020, 1960–1963, DOI: 10.1002/ejic.202000143.
30 M. Buchhorn and V. Krewald, *Dalton Trans.*, 2023, **52**, 6685–6692.
31 J. P. Snyder, *Angew. Chem., Int. Ed. Engl.*, 1995, **34**, 986–987.
32 H. B. Gray and N. A. Beach, *J. Am. Chem. Soc.*, 1963, **85**, 2922–2927.
33 A. B. P. Lever, *Inorganic Electronic Spectroscopy*, Elsevier, New York, 2nd edn, 1984.
34 G. Drabik, J. Szklarzewicz and M. Radoń, *Phys. Chem. Chem. Phys.*, 2021, **23**, 151–172.
35 V. M. Rayón and G. Frenking, *Organometallics*, 2003, **22**, 3304–3308.
36 R. J. Deeth, *Faraday Discuss.*, 2003, **124**, 379–391.
37 S. Riedel and M. Kaupp, *Coord. Chem. Rev.*, 2009, **253**, 606–624.
38 J. M. Rall, M. Lapersonne, M. Schorpp and I. Krossing, *Angew. Chem., Int. Ed.*, 2023, **62**, e202312374.
39 J. R. Winkler and H. B. Gray, in *Molecular Electronic Structures of Transition Metal Complexes I*, ed. D. M. P. Mingos, P. Day and J. P. Dahl, 2012, vol. 142, pp. 17–28.
40 M. A. Buijse and E. J. Baerends, *J. Chem. Phys.*, 1990, **93**, 4129–4141.
41 M. Kaupp, *J. Comput. Chem.*, 2007, **28**, 320–325.
42 D. W. Smith, *Inorg. Chim. Acta*, 1977, **22**, 107.
43 M. J. Riley, *Inorg. Chim. Acta*, 1998, **268**, 55–62.
44 R. J. Deeth and D. L. Foulis, *Phys. Chem. Chem. Phys.*, 2002, **4**, 4292–4297.